Hyperspectral imaging with scanning near-field optical microscopy: applications in plasmonics

J.-S. Bouillard,* S. Vilain, W. Dickson, and A. V. Zayats

Centre for Nanostructured Media, IRCEP, The Queen's University of Belfast, Belfast BT7 1NN, United Kingdom
**j.bouillard@qub.ac.uk*

Abstract: We present the realisation of near-field spectroscopic measurements with fibre-tip-based scanning near-field microscopy. It allows the simultaneous acquisition of near-field images in a broad spectral range (400 nm to 1000 nm), thus recovering local spectroscopic information. This technique is essential in order to understand the resonant interaction of light with nanostructured material as the far-field and near-field spectral response can differ significantly, e.g., in the case of plasmonic nanostructures. Several example applications of hyperspectral near-field imaging are given for visualisation of Bloch modes in plasmonic crystals and plasmon-assisted transmission through a slit.

OCIS codes: (180.4243) Near-field microscopy; (110.4234) Multispectral and hyperspectral imaging; (240.6680) Surface plasmons; (300.6550) Spectroscopy, visible.

References and links

1. L. Novotny, and B. Hecht, *Principles of Nano-optics* (Cambridge Univ. Press, 2006)
2. A. Zayats, and D. Richards, eds., *Nano-optics and Near-field Optical Microscopy* (Artech House, 2008)
3. A. A. Mikhailovsky, M. A. Petruska, M. I. Stockman, and V. I. Klimov, "Broadband near-field interference spectroscopy of metal nanoparticles using femtosecond white-light continuum," Opt. Express **28**, 1686–1688 (2003).
4. K. Karrai, and R. D. Grober, "Piezoelectric tip-sample distance control for near field optical microscopes," Appl. Phys. Lett. **66**(14), 1842–1844 (1995).
5. A. V. Zayats, I. I. Smolyaninov, and A. A. Maradudin, "Nano-optics of surface plasmon polaritons," Phys. Rep. **408**(3-4), 131–314 (2005).
6. I. I. Smolyaninov, W. Atia, and C. C. Davis, "Near-field optical microscopy of two-dimensional photonic and plasmonic crystals," Phys. Rev. B **59**(3), 2454–2460 (1999).
7. C. Ropers, D. J. Park, G. Stibenz, G. Steinmeyer, J. Kim, D. S. Kim, and C. Lienau, "Femtosecond light transmission and subradiant damping in plasmonic crystals," Phys. Rev. Lett. **94**(11), 113901 (2005).
8. W. Dickson, G. A. Wurtz, P. R. Evans, R. J. Pollard, and A. V. Zayats, "Electronically controlled surface plasmon dispersion and optical transmission through metallic hole arrays using liquid crystal," Nano Lett. **8**(1), 281–286 (2008).
9. W. L. Barnes, A. Dereux, and T. W. Ebbesen, "Surface plasmon subwavelength optics," Nature **424**(6950), 824–830 (2003).
10. S. I. Bozhevolnyi, "Near-field mapping of surface polariton fields," J. Microsc. **202**(Pt 2), 313–319 (2001).
11. S. A. Darmanyan, M. Neviere, and A. V. Zayats, "Analytical theory of optical transmission through periodically structured metal films via tunnel-coupled surface polariton modes," Phys. Rev. B **70**(7), 075103 (2004).
12. A. Drezet, D. Koller, A. Hohenau, A. Leitner, F. R. Aussenegg, and J. R. Krenn, "Plasmonic crystal demultiplexer and multiports," Nano Lett. **7**(6), 1697–1700 (2007).
13. V. Mikhailov, G. A. Wurtz, J. Elliott, P. Bayvel, and A. V. Zayats, "Dispersing light with surface plasmon polaritonic crystals," Phys. Rev. Lett. **99**(8), 083901 (2007).
14. H. J. Lezec, A. Degiron, E. Devaux, R. A. Linke, L. Martin-Moreno, F. J. Garcia-Vidal, and T. W. Ebbesen, "Beaming light from a subwavelength aperture," Science **297**(5582), 820–822 (2002).
15. E. Laux, C. Genet, T. Skauli, and T. W. Ebbesen, "Plasmonic photon sorters for spectral and polarimetric imaging," Nat. Photonics **2**(3), 161–164 (2008).

1. Introduction

Scanning near-field optical microscopy (SNOM) is an important tool for modern nano-optical and nanophotonic studies allowing nanoscale field mapping around nanostructured materials and in micro- and nanoscale devices [1,2]. Knowledge of local electromagnetic field distributions combined with a simultaneously acquired topography of the surface, as common

#127481 - $15.00 USD Received 26 Apr 2010; revised 13 Jun 2010; accepted 13 Jun 2010; published 21 Jul 2010

in SNOM, is imperative to understand nanoscale light-matter interactions in various nanostructured material systems and nanolocal optical characterization of materials. Direct comparison of the electromagnetic field distribution and topography thus enables realistic association with model calculations.

In most cases SNOM measurements are restricted to wavelengths provided by available laser sources. At the same time, the studied objects may exhibit strongly resonant optical behavior, with optical properties crucially depending on the wavelength of the excitation light. These may be quantum dots, molecules, plasmonic and photonic nanostructures and metamaterials. Moreover, the resonant wavelength position may be strongly modified due to the electromagnetic interaction between the objects, so it is not always possible and straightforward to predict it even if the resonant optical properties of individual objects are known. In this case during SNOM measurements with a fixed illumination wavelength, the spectral behavior and resonant properties of the objects are completely hidden.

In the past, even if the spectral dependence of SNOM images has been studied, it was done in a sequential manner by recording several consecutive SNOM images obtained using a different illumination wavelength, or by sequentially taking a spectrum at a few specific points of the image [3]. This approach is very time consuming and suffers from system drifts as well as sample and tip deterioration from scan to scan as multiple images are required.

In order to overcome these difficulties and introduce real spectroscopic capabilities in scanning near-field optical microscopy we have developed a hyperspectral scanning near-field optical microscope capable of recording, simultaneously, multiple near-field images in 400—1000 nm spectral range during a single scan. This provides access to the near-field spectroscopic properties of nano-objects and enables direct comparison of the images obtained at different wavelengths under exactly the same sample and tip conditions and drift-free. In the following, we will describe the principles of the hyperspectral SNOM imaging and present several example applications of the instrument to imaging of plasmonic structures for which near-field spectroscopy is imperative for clarifying the underlying physical processes.

2. Experimental set up

The SNOM instrument used for hyperspectral imaging is based on metal coated optical fibre probes with a nano-aperture at the tip. This allows measurements in either illumination mode, when white light is sent through the SNOM probe or in collection mode when the probe is collecting the light after its interaction with the sample (Fig. 1). The probe is mounted on a piezo-tube, for z-direction control, which is in turn mounted on a 2D piezo-stage to scan the probe in the x and y directions parallel to the sample surface. In the alternative configuration, the sample is mounted on the 2D piezo-stage and scanned with respect to the tip.

The tapping-mode distance regulation system is based on the quartz tuning fork to which the probe is attached [4]. A frequency generator is used to excite the tuning fork-fibre system at its resonance frequency, around 32.7 kHz (tuning forks dependent), and the current flowing through the tuning fork is monitored. As the probe is approached to the sample, the oscillations of the tuning fork are increasingly damped due to the dispersive surface forces acting on the tip of the probe. During scanning, this feedback signal is maintained at constant amplitude using the z-distance control, generating the topographic image.

SNOM probes are fabricated using pulled optical fibre which are then bent at around 90° (Fig. 1 (b)) enabling the implementation of tapping mode distance regulation. The SNOM probes used were made using telecom optical fibre with a 9 μm core. The fibre is first stretched in order to taper it at one end and is then bent at 90° by thermal heating using a fibre splicer. The fibre tip can be metal coated if desired. For the metal coated probes, gold is sputtered onto a rotating fibre tip; a nano-aperture is then formed by cutting the extremity of the probe at 90° using Focussed Ion Beam (FIB). Depending on the position where the SNOM probe is cut, apertures between 50 nm and 500 nm diameter can be reproducibly obtained. An example of such nano-aperture is shown on the SEM image in Fig. 1 (c).

For near-field spectroscopy, coherent broadband light (400 nm to 1000 nm wavelength) from a supercontinuum laser source is used to illuminate the sample. The light from the laser

#127481 - $15.00 USD Received 26 Apr 2010; revised 13 Jun 2010; accepted 13 Jun 2010; published 21 Jul 2010

is first injected into an endlessly monomode photonic crystal fiber in order to localize all the wavelengths in a single Gaussian spot. One can either illuminate the sample locally by coupling light into the SNOM probe with detection in the far field using a microscope objective or illuminate the sample from the far-field and detect the signal in the near-field via the SNOM probe. In either case, the detected light is spectrally separated by a spectrometer coupled to a high speed CCD. A full spectrum is acquired at each pixel of the SNOM image, therefore generating the multispectral near-field optical response of the sample.

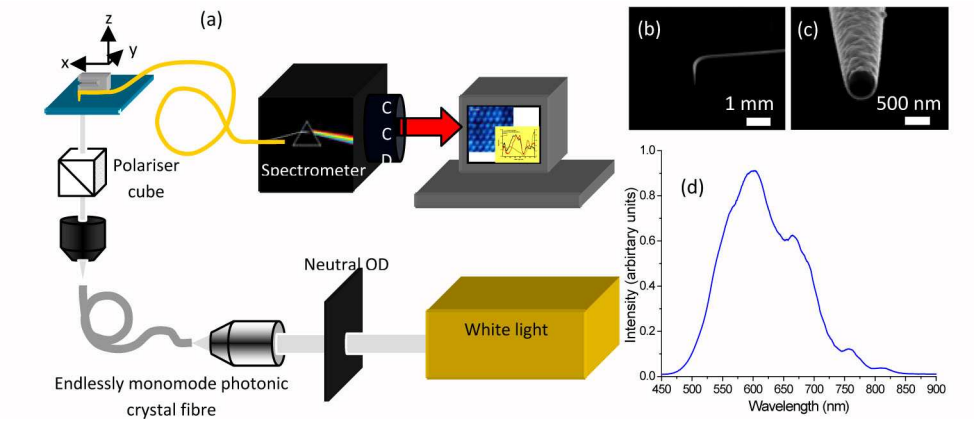

Fig. 1. (a) Schematic of the SNOM setup with integrated spectroscopy. (b) Optical and (c) SEM images of the metal coated fiber probe tip. (d) Typical spectral sensitivity of the SNOM set-up is a convolution of the transmission spectrum of the SNOM fiber probe tip, sensitivity of the spectrograph and CCD as well as the spectrum of the illuminating light.

Each image is typically taken at a scan rate of 0.1 Hz (for one trace and retrace cycle) with 256 lines per image and 256 points per line. This means that each image contains 131072 pixels (counting the trace and retrace for one scan), and the same number of spectra are recorded. The acquisition time per pixel is approximately 20 ms which determines the integration time of the spectra. This time was experimentally fine tuned to compensate for the inaccuracy of the various synchronization devices. After image acquisition, each spectrum is normalized to the reference spectrum (Fig. 1 (d)) taking into account background signal level.

The resulting data set is usually processed to create a false movie describing the evolution of the near-field distribution on the surface of the sample as the wavelength changes. Each snap-shot of the movie corresponds to a near-field image at a given wavelength. Since all such images are acquired simultaneously during the same scan, they can be directly compared as there are no drifts or shifts between the individual images. One can also extract the local near-field spectra at any point of the image if desired. As in conventional SNOM, the associated, simultaneously measured topographic image is readily available to compare with the optical images.

3. Application examples

In this section results are presented illustrating several highly relevant applications of near-field spectroscopy in the field of nano-optics and plasmonics demonstrating the potential of the developed technique. These clearly show differences in the far-field and near-field spectral response of the plasmonic nanostructures illustrating that knowledge of near-field spectral behavior is imperative for interpreting the underlying physical mechanisms.

3.1 Imaging SPP Bloch modes in plasmonic crystals

Periodically nanostructured metal films or surfaces act as plasmonic crystals for surface plasmon polaritons (SPPs) in analogy to 2D photonic crystals [5–9]. The interaction of SPPs with a periodic structure leads to a modification of the SPP dispersion compared to an unstructured metal film, resulting in the formation of forbidden and allowed bands. In the

#127481 - $15.00 USD Received 26 Apr 2010; revised 13 Jun 2010; accepted 13 Jun 2010; published 21 Jul 2010

latter, SPP Bloch modes are supported by the periodic structure. These modes determine the optical properties of structured metal films such as transmission, reflection and absorption. Usually, the optical properties of plasmonic crystals have been studied in the far-field by measuring their far-field transmission or reflection [5,8]. The hyperspectral SNOM described above can be used to study the near-field transmission of the crystal and directly visualize the field distribution of the supported SPP Bloch modes.

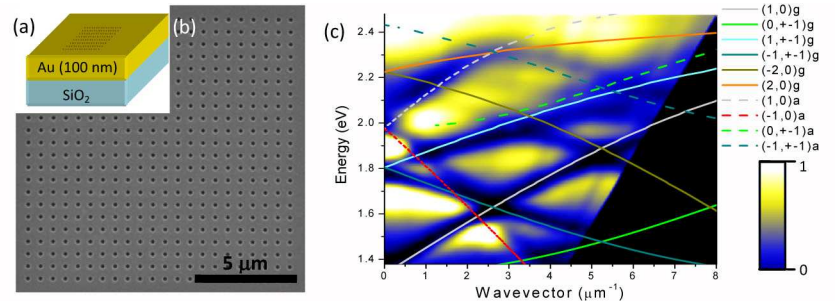

Fig. 2. (a) Schematic and (b) SEM image of the plasmonic crystal used in the experiments: Au film is 100 nm thick, the holes diameter is 200 nm, the array period is 600 nm, the overall size of the array is 10x10 µm^2. (c) Far-field transmission dispersion of the crystal measured with p-polarised incident light. Lines show the spectrum of the Bragg-scattered SPPs calculated using the SPP modes on the smooth Au surface [8]. $(p,q)_g$ denotes the glass-Au modes and $(p,q)_a$ denotes air-Au modes.

Initially, the Bloch modes of a SPP crystal (SPPC) consisting of a square array of circular holes were studied (Fig. 2). The near-field spectra and the spatial variations of the near-field intensity at different wavelengths measured with the hyperspectral SNOM are presented as the false movie (Media 1). Snapshots taken from the movie for several wavelengths and near-field spectra at certain points on the SPPC are presented in Fig. 3.

For wavelengths shorter than 500 nm, a grid like distribution of the field is observed with a period of 600 nm. The bright spots correspond to the direct transmission through the holes of the structure since, due to optical properties of Au, no SPPs are excited at those wavelengths. For longer wavelengths, the field distribution changes to lines perpendicular to the polarization of the incident light. Those are the expected Bloch modes of a square lattice arising from the 1st-order Bragg scattering of the SPP by the holes in the array in the Γ-X direction of the Brillouin zone [5,8,11]; cf. Bloch modes around the band gaps 1.9—2.1 eV at k = 0 in Fig. 2 (c). These are the SPP Bloch modes at the Au-air interface. Please note that due to the dominant sensitivity of the SNOM fiber probe to E_x component of the electric field of the SPP mode [10], the presented images reflect the $|E_x|^2$ distribution, rather than total SPP intensity and thus have the period of the crystal lattice (Fig. 3 (k)) [11]. When frequency is scanned across the band-gap, the field distribution of the Bloch modes existing at the opposite edges of the band-gap are shifted with respect to the elementary cells of the lattice having maxima between the holes or at the hole sites at different band edges (Fig. 3 (k), cf also (d) and (g)) [5,11]. One can also notice the complex field pattern (Fig. 3 (e), (f)) where the contribution of the third mode become noticeable probably due to a slight non-perfect collimation of the illuminating light. The influence of the lowest Γ-M mode on the Au-substrate interface and other interface modes are visible in Media 1, but their relative intensity is much smaller than that of the Au-air modes.

The observed near-field spectra at different points above the surface (Fig. 3 (j)) show generally the same spectral features but their relative weight depends on the position above the surface, e.g., different transmission peaks are related to different SPP Bloch modes. The features due to the transmission directly through the holes are less pronounced, as should be expected, as well as are the glass-Au SPP modes. The near-field distributions mainly follow the Bloch mode pattern on the air-Au interface.

#127481 - $15.00 USD Received 26 Apr 2010; revised 13 Jun 2010; accepted 13 Jun 2010; published 21 Jul 2010

3.2 SPP Bloch mode refraction at the crystal boundary

Having visualized the SPP Bloch modes within the crystal, it is interesting to see their modifications near the crystal boundary. Strictly speaking, Bloch modes are defined for an infinite periodic structure. The influence of the finite-size crystal will be in the reflection and refraction of the modes on the crystal boundary where periodicity is broken [12,13]. These processes result in the modification of the field distribution both within the crystal, due to the presence of additional interfering waves after reflection from the crystal boundary inside

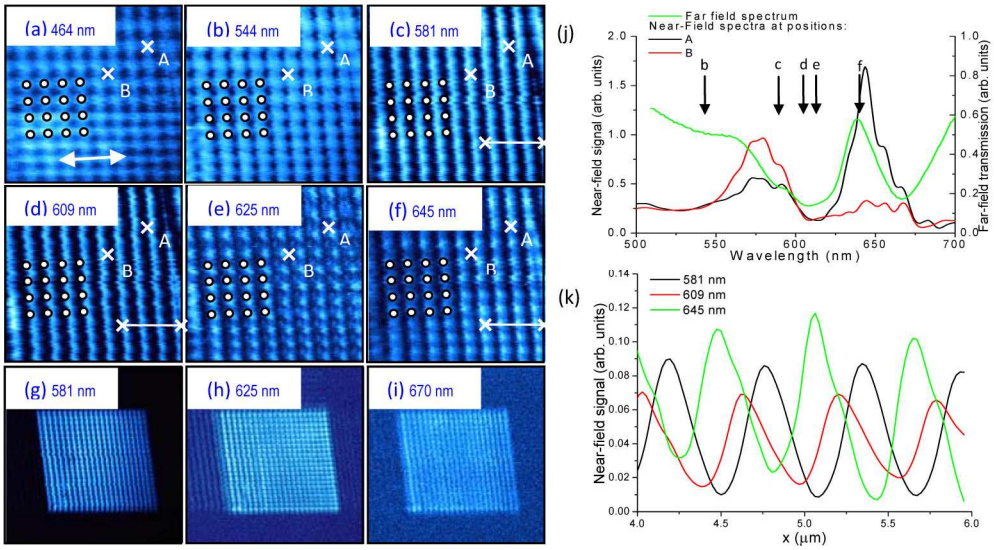

Fig. 3. (a-f) Near-field intensity distributions measured above the SPP crystal surface at different wavelengths (snapshots reconstructed from Media 1). The image (6x6 μm^2 size) is obtained with the SNOM in collection mode under far-field illumination at normal incidence. (g-i) Near-field intensity distributions measured above the metal surface at different wavelengths (snapshots reconstructed from Media 2). The image size is 50x50 μm^2. (j) Far-field and near-field transmission spectra of the SPP crystal. The near-field spectra are reconstructed from Media 1 at the positions A and B, respectively: A is above a hole and B is between holes. The wave length at which the images are presented in (a-f) are indicated by arrows. (k) Profiles of the Bloch mode field measured from the near-field optical images for the wavelengths of 581 nm, 609 nm and 645 nm along the line indicated in (c,d,f). The polarization of the illuminating light is indicated in (a).

SPPC, as well as outside the crystal boundary, where smooth film SPPs can appear after the Bloch modes are refracted from the crystal onto the smooth surface.

The evolution of the near-field intensity distribution on the surface outside the crystal for varying incident light wavelengths is shown in Media 2. Snapshots of the movie at the selected wavelengths (Fig. 3 (g-i)) show the SPP waves being launched from the plasmonic crystal boundaries onto the smooth gold film. As discussed above, the asymmetry in the interference pattern on Fig. 3 (g-i) arises from a slightly non-perfect collimation of the illuminating light. Once again we would like to stress that all those images are snapshots recovered from the same optical data file and were all acquired simultaneously. One can see that when smooth film SPP's are launched, the field intensity distribution above the structured area is changed in the same way as when crossing of the bandgap (Fig. 3 (c,e)). This is related to the fact that the excitation conditions for smooth film SPPs coincides exactly with the band-gap of the SPP crystal [5,13].

3.3 Near-field spectroscopy of the transmission through a single slit

In the photo-detector industry, there is a great need to reduce the size of the active area of photodetectors without reducing their efficiency. This may be accomplished by employing

#127481 - $15.00 USD Received 26 Apr 2010; revised 13 Jun 2010; accepted 13 Jun 2010; published 21 Jul 2010

light gathering structures, consisting of a one dimensional surface grating with a single central aperture or slit commonly termed a 'slit and grooves' structure [14,15]. Such structures, when illuminated at the edge of the band-gap, couple the incident light to SPP Bloch modes which propagate towards the slit aperture and are transmitted through it. The transmitted light spectrum is determined by the dispersion of the grating and transmission of the slit [15]. The resulting far-field transmission exhibits highly selective wavelength dependence and is therefore ideally suited to investigation using hyperspectral SNOM imaging.

The structures were studied using the hyperspectral SNOM operating in illumination mode: incoming light is coupled into the optical fibre of the SNOM probe and the gold coated tip is used to locally illuminate each point of the structure in the near-field. Local illumination provides information on how each part of the structure contributes to the signal transmitted through the central slit (Media 3).

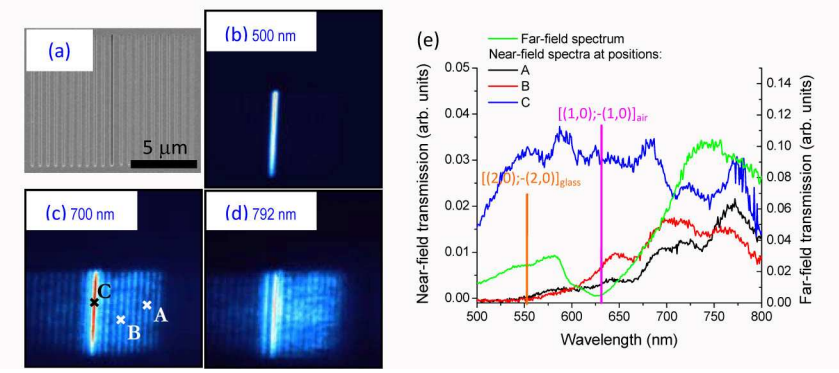

Fig. 4. (a) SEM image of the slit-and-grooves structure: the grooves are 50 nm deep and 100 nm wide and have a period of 600 nm, and the central slit is 100 nm wide; the Au film is 300 nm thick; 10 grooves have been fabricated on each side of the slit with some asymmetry. (b-d) The images of the near-field coupling efficiency measured above the SPP crystal surface at different wavelengths (snapshots reconstructed from Media 3). (e) The transmission spectra measured with far-field and near-field illumination of the structure. The near-field spectra are reconstructed from Media 3 at the positions A, B and C, respectively. The normalization is internal for each spectrum.

Notwithstanding the transmission of the slit, a transmission maximum should be expected at the band edge of the periodic grooves where coupling to SPP's is most efficient (see section 3.1). This is confirmed by examining the transmitted light when only the slit is illuminated. The broad featureless nature of the spectrum demonstrates the absence of slit resonances in this spectral range, such as Fabry-Perot resonances or cut-off of the waveguided modes (Fig. 4 (e)). When the grating is illuminated, a clear spectral dependence arises due to the light coupling into SPP modes on the grating, with the local maximum near the same wavelength as in the far-field transmission spectrum. This can be confirmed by the dependence of the transmission spectrum on the position of the illuminating probe. The further the tip from the slit, the more red-shifted the transmission peak due to the decrease of the propagation length of SPPs as the illuminating wavelength decreases, i.e., the further the tip from the slit, the smaller the contribution of shorter wavelengths since their propagation length is smaller. The role of the SPP excitation is also evident from the near-field distributions at different wavelengths corresponding to the different sides of the band-gaps of the grating (cf. Figure 4 (c) and (d)). When no SPPs are excited, at wavelengths below 550 nm, due to the optical properties of Au, only direct transmission through the slit is important (Fig. 4 (b)).

4. Conclusions

We have described the implementation of near-field spectroscopic measurements using a SNOM set-up combined with white-light illumination and spectrally sensitive detection. It allows investigation of the spectral optical properties of the samples of interest at every point

#127481 - $15.00 USD Received 26 Apr 2010; revised 13 Jun 2010; accepted 13 Jun 2010; published 21 Jul 2010

of the SNOM image therefore enabling reconstruction of resonant near-field optical properties of the object which can significantly differ from the far-field optical properties. The power of this approach has been demonstrated in several examples addressing different properties of plasmonic structures. Comparison of the near- and far-field spectral response and spectral dependence of the near-field distributions provide important insights into underlying physics and details of the interaction of light with nanostructured surfaces can be unambiguously identified.

Acknowledgments

This work was supported by the FP6 STREP PLEAS. A. Zayats, W. Dickson, and S. Vilain acknowledge the financial support from EPSRC (UK). The authors thank Regis Deturche from the LNIO (Troyes, France) for discussion of the SNOM feedback system.

#127481 - $15.00 USD Received 26 Apr 2010; revised 13 Jun 2010; accepted 13 Jun 2010; published 21 Jul 2010